THE JOURNAL OF PHYSICAL CHEMISTRY C
A JOURNAL OF THE AMERICAN CHEMICAL SOCIETY

pubs.acs.org/JPCC
Article

Galvanic Displacement Reaction Enabled Specific and Sensitive Detection of Bacteria with a Digital Photocorrosion GaAs/AlGaAs Biosensor

Amanpreet Singh, Walid M. Hassen, René St-Onge, and Jan J. Dubowski*

Cite This: J. Phys. Chem. C 2023, 127, 21768−21776
Read Online

ACCESS | Metrics & More | Article Recommendations | Supporting Information

ABSTRACT: The conjugation of ionic gold with bacterial antibodies makes it possible to induce a specific interaction between targeted bacteria and the surface of a GaAs/AlGaAs biochip. The process of immobilization is based on a galvanic displacement reaction (GDR) involving electron transfer between GaAs and Au^{3+} ions that leads to the formation of a Au−Ga alloy anchoring bacteria to the biochip surface. The GDR-based immobilization of *Escherichia coli* on biochips comprising a stack of GaAs/AlGaAs nanolayers (d_{GaAs} = 12 nm, d_{AlGaAs} = 10 nm) was confirmed by X-ray photoelectron spectroscopy and atomic force microscopy-based infrared experiments. We report the successful application of this approach for highly sensitive detection of *E. coli* with a digital photocorrosion (DIP) biosensor. The photoluminescence (PL) monitored DIP of GaAs/AlGaAs nanolayers results in the formation of a PL intensity maximum whose temporal appearance depends on the electric charge transfer between bacteria and the biochip. The formation of a robust bacteria−biochip interface achieved with the GDR process allowed us to observe the role of bacteria on the temporal position of a PL intensity maximum related to the etching of two pairs of GaAs/AlGaAs nanolayers extending up to 24 nm below the biochip surface. We demonstrate the attractive detection of *E. coli* at 250 CFU/mL, and we discuss the potential of this approach for designing a family of biosensors addressing the quasi-continuous monitoring of a water environment for the presence of pathogenic bacteria.

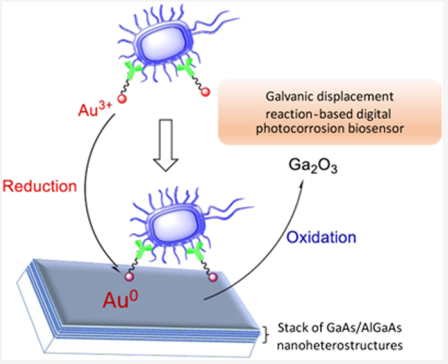

1. INTRODUCTION

Due to the contamination of groundwater sources and the growing water consumption related to human needs and activities, providing clean water to large populations is a major challenge for agricultural, industrial, and municipal entities.[1−3] Although the majority of bacterial strains are not harmful and some bacteria are involved in the digestion of food and other biological transformations,[4−6] other bacteria are the source of common human illnesses and can cause severe infections.[7−9] Thus, monitoring pathogenic bacteria is vitally important for minimizing human health risks.[10−13] There are numerous well-established biosensing techniques, such as nucleic acid polymerase chain reaction (PCR),[14,15] antibody/antigen enzyme-linked immunosorbent assay (ELISA),[16−19] or matrix-assisted laser desorption ionization mass spectroscopy (MALDI-TOF)[20] that allow attractive sensing with a limit of detection (LOD) ranging from 1 to 10 CFU/mL, or even better.[21−26] However, these techniques are based on laboratory settings, suffer from a relatively long analysis time, and are not easily adaptable to automated or quasi-continuous monitoring.[27] A plethora of electrochemical,[28] optical,[29] and field-effect[30] biosensors has been investigated to address the problem of sensitive detection potentially out of laboratory settings. In that context, detection of bacteria even with a relaxed LOD but relatively close to the infective dose would be attractive for prescreening of water samples from rivers, lakes, industrial waste, or sewage systems if delivered quasi-continuously and at an attractive cost. Such an approach would be of importance to early detection and prevention of outbreaks of infections potentially leading to pandemic situations.

Recently, we introduced the innovative technology of digital photocorrosion (DIP) biosensing employing devices comprising GaAs/AlGaAs nanoheterostructures.[31−33] This method is based on monitoring the process of DIP with the photoluminescence (PL) effect, which reveals PL intensity maxima formed as the photocorrosion front passes through a pair of GaAs/AlGaAs (d_{GaAs} = 12 nm, d_{AlGaAs} = 10 nm) nanolayers.[34,35] The process is sensitive to the flow of electric charge between immobilized bacteria and the semiconductor surface, which affects DIP rates and allowed for rapid and sensitive detection of *Escherichia coli*[32,36] and *Legionella pneumophila*.[31,33,37,38] The biosensing results were obtained

Received: August 2, 2023
Revised: October 12, 2023
Accepted: October 13, 2023
Published: October 29, 2023

by employing antibodies[32,36,37,39,40] and antimicrobial peptides.[33,38,41] The sensitivity of DIP biosensing is analogous to the sensitivity of plasmonic and nanoparticle devices to charge transfer based on the galvanic displacement reaction (GDR).[42−44] Owing to the large gap between the reduction potentials of GaAs and Au^{3+} ions, the GDR process is triggered by spontaneous electron transfer.[45,46] Consequently, GaAs is oxidized, and the Au^{3+} ions are reduced to Au^0. This results in the formation of a Au−Ga alloy at the interface of GaAs with Au^0 nanoparticles as reported earlier by Sayed et al.[47] Previously, we explored the GDR-based process for microscopic imaging of *L. pneumophila* decorated with Au^0 nanoparticles without the need for employing dyes or green fluorescent proteins normally applied for enhancing bacterial imaging.[48]

In this study, we investigate the innovative concept of DIP biosensing based on the application of GaAs/AlGaAs chips with an unfunctionalized surface. The GDR-based formation of robust bacteria−biochip hybrids allowed observation of photocorrosion continuing through a set of two pairs of GaAs/AlGaAs nanolayers, which resulted in a significantly enhanced LOD. We also discuss the advantage of this approach for designing regenerable biosensors comprising stacks of GaAs/AlGaAs nanoheterostructures.

2. MATERIALS AND METHODS

2.1. Materials. Mercaptohexadecanoic acid (MHDA), *N*-hydroxy succinimide (NHS), gold chloride ($AuCl_3$), 1-ethyl-3-(3-(dimethylamino)propyl)carbodiimide (EDC), agar, and Luria−Bertani (LB) medium were purchased from Sigma-Aldrich (Oakville, ON, Canada) and used without further purification. All of the employed solvents were of spectroscopic grade. Unconjugated polyclonal antibodies (pAbs) against *E. coli* were obtained from Virostat Inc. Portland (Maine, USA). Green fluorescent *E. coli* K12 BW25113 (GFP *E. coli*) was obtained from the Department of Microbiology and Infectiology of the Université de Sherbrooke (UdS) Faculty of Medicine (Sherbrooke, QC, Canada), and *Pseudomonas aeruginosa* ATCC 27853 (*P. aeruginosa*) was obtained from the Department of Biology of the UdS Faculty of Sciences (Sherbrooke, QC, Canada).

2.2. GaAs/$Al_{0.35}Ga_{0.65}As$ Nanoheterostructures. Nanoheterostructures (Wafer D3422) were grown by metal−organic vapor phase epitaxy on a semiinsulating GaAs (001) substrate. They consist of a 20-pair AlAs/GaAs (2.4/2.4 nm) superlattice and a 500 nm GaAs buffer layer followed by a 100 nm-thick $Al_{0.35}Ga_{0.65}As$ layer and six pairs of 12 nm-thick GaAs and 10 nm-thick $Al_{0.35}Ga_{0.65}As$. The microstructure was capped with a 12 nm-thick GaAs layer. The 2 × 2 mm chips were prepared by dicing the original wafer and cleaning it with an ultrasonic bath using acetone, OptiClear, acetone, and isopropanol sequentially for 5 min each. The final step included etching in 28% NH_4OH for 2 min at room temperature to remove native oxides from the surface of the GaAs.

2.3. Functionalization of *E. coli*. In 0.8 mL of ethanol/1× PBS (50:50, *v*/*v*), 5 μL of 10 mM $AuCl_3$ in DI water was mixed with 5 μL of 10 mM MHDA in ethanol. After 15 min, 3.8 mg (2 mM) of EDC was added to the above solution followed by the addition of 1.5 mg of NHS. The mixture was kept for 20 min, and then, 20 μL of a 4 mg/mL solution of unconjugated pAbs against *E. coli* was added. Next, 1 mL of the solution was prepared by the addition of 1× PBS. After 1 h, either *E. coli* (positive test) or *P. aeruginosa* (negative test) suspension at 10^8 CFU/mL (0.1 $OD_{600\ nm}$ corresponds to 10^8 and 2 × 10^7 CFU/mL, respectively, for *E. coli* and *P. aeruginosa*) prepared from pure fresh cultures in the LB agar medium was added to the mixture and incubated for 20 min.

Suspensions of bacteria decorated with Ab−Au^{3+} hybrids were prepared in PBS (1×, 7.4 pH) and flowed through the flow cell for 20 min. Next, the flow was stopped for 5 min to allow the bacteria to deposit on the biochip surface, and DI water was used to remove loosely bonded analytes from the biochip surface. The photocorrosion of GaAs/AlGaAs nanoheterostructures was carried out under continuous flow of DI water at 0.04 mL/min and monitored with the photoluminescence originating from GaAs layers.

Note: For a higher concentration of gold employed for decoration of 10^8 CFU/mL *E. coli*, the concentration of EDC, NHS, and MHDA was multiplied by the same number as that of the gold ion.

2.4. Fourier Transform Infrared Spectroscopy Analysis. FTIR absorption spectroscopy measurements were performed by using a Bruker Optics Hyperion 2000 FTIR system. The spectra were collected at a resolution of 4 cm^{-1} and averaged over 1000 scans. All FTIR data were recorded using a liquid N_2 chilled HgCdTe (mercury cadmium telluride) IR detector. A reference GaAs sample was obtained by consecutive cleanings in ultrasound baths with OptiClear, acetone, isopropanol, acetone, and ethanol (5 min each) and then etched with a 28% NH_4OH solution. The samples with undecorated and Ab−Au^{3+}-decorated *E. coli* were prepared by placing ∼10^6 bacteria on the surface of etched 4 mm × 4 mm GaAs and letting it dry for 2 h.

2.5. Photoluminescence Measurements. Time-dependent PL intensity was measured using a custom-designed quantum semiconductor photonic biosensor reader (QSPB-2).[34] Unless indicated otherwise, the samples were irradiated with 1.8 s pulses every 25 s (DC = 1.8/25) using a homogenized beam of the light-emitting diode operating at 660 nm and delivering a power of 15 mW/cm^2 to the sample surface.

2.6. X-ray Photoelectron Spectroscopy Characterization. X-ray photoelectron spectroscopy (XPS) measurements were performed by using a Kratos Analytical AXIS Ultra DLD XPS spectrometer equipped with an Al Kα source operating at 150 W. The GaAs/AlGaAs nanoheterostructures were exposed for 20 min to gold-functionalized bacteria, and XPS measurements were conducted in the Au 4f, Ga 3d, C 1s, and As 3d transition regions to investigate the chemical composition of the GaAs substrate after completing the GDR step. Data were collected at a takeoff angle of 60° with respect to the surface normal.

2.7. Atomic Force Microscopy. The surface morphology of the processed samples was studied by using atomic force microscopy (AFM, Digital Instruments, Nanoscope). The AFM instrument was operated in tapping mode. All images were collected over a 1.0 μm × 1.0 μm surface area with 512 scans using a tip velocity of 1 μm/s and at a scan rate of 0.5 Hz.

2.8. AFM-IR. Atomic force microscopy-based infrared (AMF-IR) spectra were recorded using an AFM NanoIR2 upgraded to NanoIR3 with a QCL pulse laser (mIRCAT, Bruker, Santa Barbara) operating in the 911−1900 cm^{-1} range and employing an AFM PR-EX-nIR2 probe. The repetition rate of the QCL was tuned to match the resonant frequency mode of the Au-coated AFM cantilever in contact with the

https://doi.org/10.1021/acs.jpcc.3c05200
J. Phys. Chem. C 2023, 127, 21768−21776

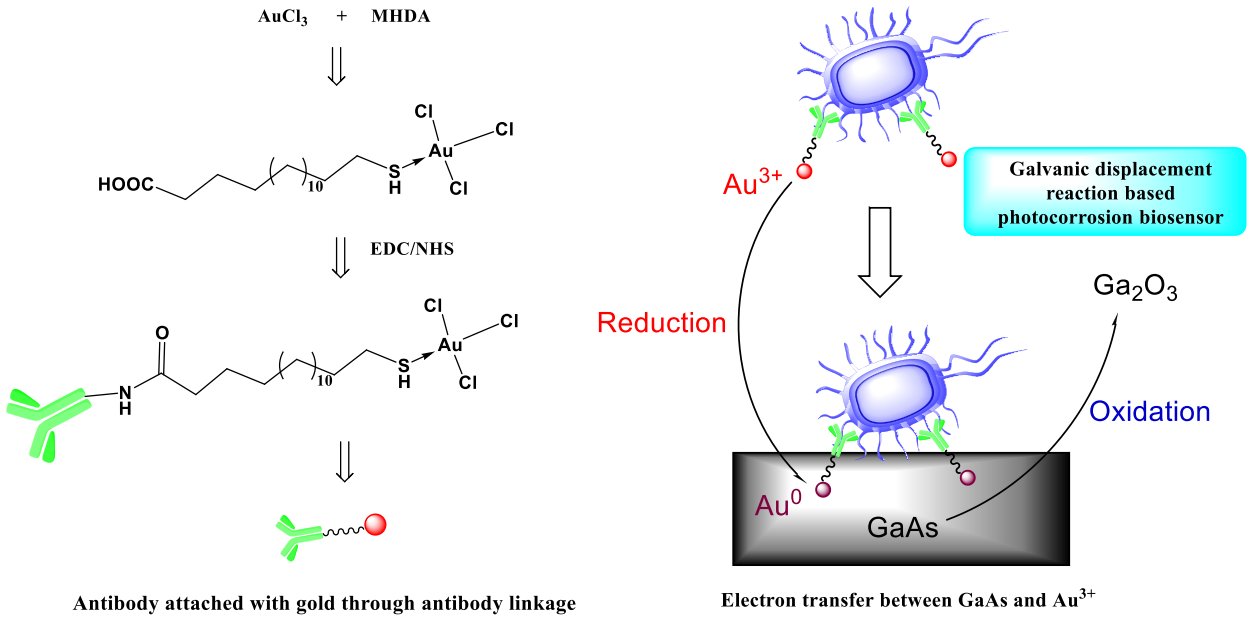

Figure 1. Graphical illustration of the mechanism of the specific absorption of gold-antibody-decorated bacteria on the GaAs surface.

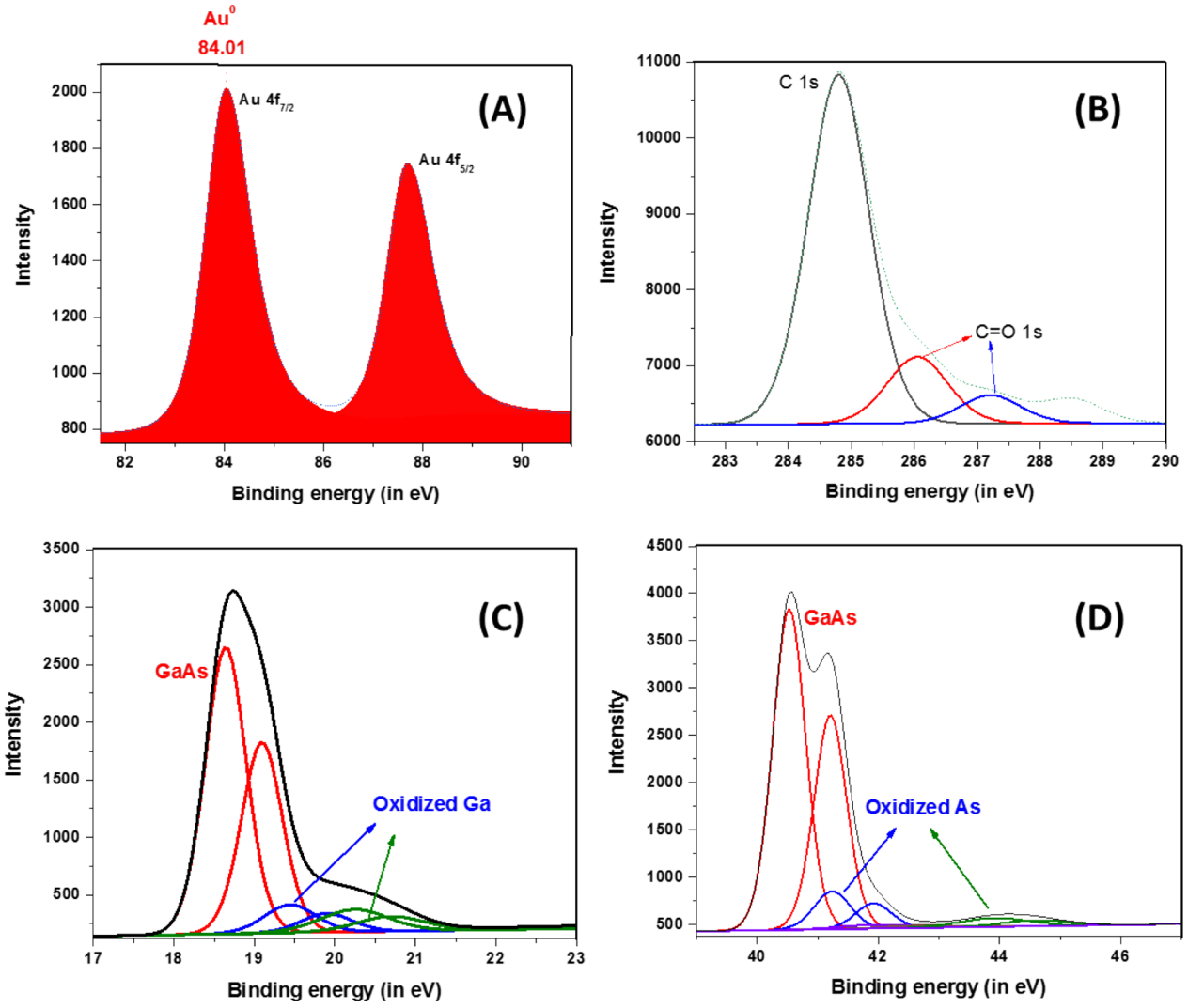

Figure 2. High-resolution XPS scans of the GaAs/AlGaAs nanoheterostructure after absorption of Au−Ab gold-coated bacteria corresponding to (A) Au 4f, (B) C 1s, (C) Ga 3d, and (D) As 3d peaks.

https://doi.org/10.1021/acs.jpcc.3c05200
J. Phys. Chem. C 2023, 127, 21768−21776

sample surface. IR spectra were collected at a spatial resolution of approximately 25 nm × 25 nm. Samples with undecorated and Ab−Au^{3+}-decorated *E. coli* were prepared by placing a 10 μL drop of bacteria from 10^4 CFU/mL suspensions on the surface of an etched 2 mm × 2 mm GaAs/AlGaAs chip and letting it dry for 2 h.

3. RESULTS AND DISCUSSION

The process of specific deposition of *E. coli* on the biochip surface is schematically shown in Figure 1 (for more details, see Figure S1). Following the formation of $AuCl_3$-Ab hybrids, an 80 μg/mL Au−Ab solution was mixed with *E. coli* suspensions at 10^8 CFU/mL. After 20 min, the functionalized bacteria were separated by centrifugation at 1000 rpm for 20 min. Subsequently, the pellet was resuspended in PBS and this mother suspension was used to carry out successive dilutions for DIP-GDR detection. Freshly etched GaAs/AlGaAs chips were exposed to Au−Ab-functionalized bacteria for 20 min and washed with DI water to remove loosely bonded products. The mechanism underlying the attachment of bacteria to the GaAs/AlGaAs biochip surface takes advantage of the significant difference between the reduction potentials of Ga and Au^{3+}. This is the result of spontaneous electron transfer from Ga(0) to Au(III), reduction of Au(III) to Au(0), and oxidation of Ga(0) to Ga(III). The Ga^{3+} ion has a more electropositive character than Au^0 according to the following process:[49]

$$Au^{3+} + 3e^- \rightarrow Au(S) \quad E_0 = +1.68V \tag{R1}$$

$$Ga(S) \rightarrow Ga^{3+} + 3e^- \quad E_0 = -0.56V \tag{R2}$$

The gold ion is converted into Au^0 and deposited over the GaAs surface along with the bacteria. An alternative mechanism of bacterial immobilization would require breaking the Au−S bond of the $AuCl_3$-MHDA complex and forming a new Ga−S bond. In this way, thiol directly attaches to the GaAs surface, promoting the direct deposition of bacteria on the GaAs surface, while the remaining gold is converted into Au nanoparticles.

The XPS spectra collected after the absorption of Au−Ab-coated bacteria on GaAs revealed the reduction of gold ions (Au^{3+}) into gold nanoparticles (Au^0) through GDR. As shown in Figure 2A, binding energies at 84.01 and 87.72 eV represent the $4f_{7/2}$ and $4f_{5/2}$ peaks of Au^0, respectively. The significant amounts (more than 75%) of C (Figure 2B), as well as N-, O-, and Cl-related compounds (Figure S2), are consistent with the presence of bacteria on the GaAs surface. It is worth mentioning that Au^0 constitutes only 0.85% of the total material on the GaAs surface, which is consistent with gold acting as a binding unit between GaAs and bacteria. In addition, as shown in Figure 2C, the XPS peaks in the Ga 3d and As 3d regions are related to the major composition of GaAs, along with Ga and As oxidized through the GDR process. In addition, the FTIR absorbance spectra of the GaAs samples exposed to *E. coli* and Au−Ab-functionalized *E. coli* from 10^8 CFU/mL suspensions showed an amide peak at 1657 cm^{-1} (Figure S3), corresponding to the C═O bond (amide I) originating from the antigen and/or antibodies,[50] consistent with the presence of bacteria on the GaAs surface.

The high spatial resolution AFM-IR experiments indicated that the position of the peak varied, depending on the point of interrogation of a bacterium. Examples of IR plots for the samples exclusively with *E. coli* and with Au^0-decorated bacteria are shown in Figure 3a and Figure 3b, respectively.

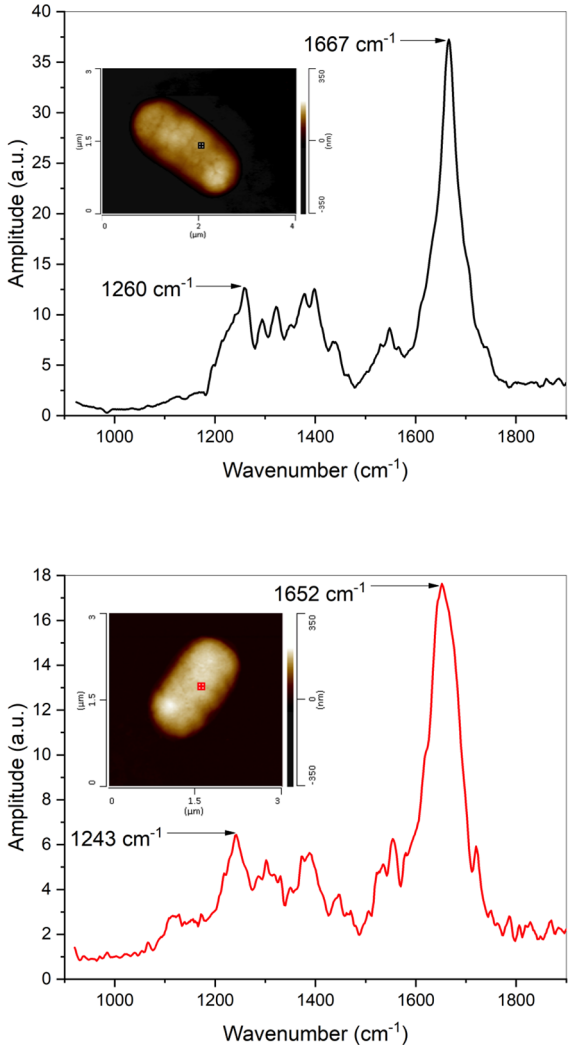

Figure 3. FTIR spectra of (top) clean *E. coli* taken at the indicated location of the 3 μm × 4 μm inset with the AFM image of a bacterium and (bottom) Au-coated *E. coli* taken at the indicated location of the 3 μm × 3 μm inset with the AFM image of a bacterium.

In addition to amide I observed between 1652 and 1667 cm^{-1} for either clean or Au^0-decorated bacteria, these results also revealed amide II and amide III features in the 1540−1558 and 1242−1260 cm^{-1} regions, respectively. The energy of the amide I feature observed at 1652 cm^{-1} is close to the *E. coli* absorption at 1653 cm^{-1} and BSA absorption at 1654 cm^{-1} observed with high-resolution FTIR spectroscopy.[50,51] Our FTIR absorption experiments indicated the increased amide II and amide III wavenumbers for Au^0-decorated bacteria, although the small data statistics of the AFM-IR measurements did not allow us to conclude anything about the systematic difference between IR data for clean and Au^0-decorated bacteria. The slightly increased wavenumbers of the amide peaks were suggested to be related to the modified conformational order of bacterial proteins resulting from interaction with solid substrates.[52,53]

The GDR-based immobilization of Ab-ionic gold-decorated bacteria allowed for the observation of a decreased photocorrosion rate of GaAs/AlGaAs chips owing to the flow of an extra negative charge to the chip surface. Examples of the PL intensity plots recorded for a reference DIP run in DI water and for bacterial suspensions ranging between 250 and 10^4

https://doi.org/10.1021/acs.jpcc.3c05200
J. Phys. Chem. C 2023, 127, 21768−21776

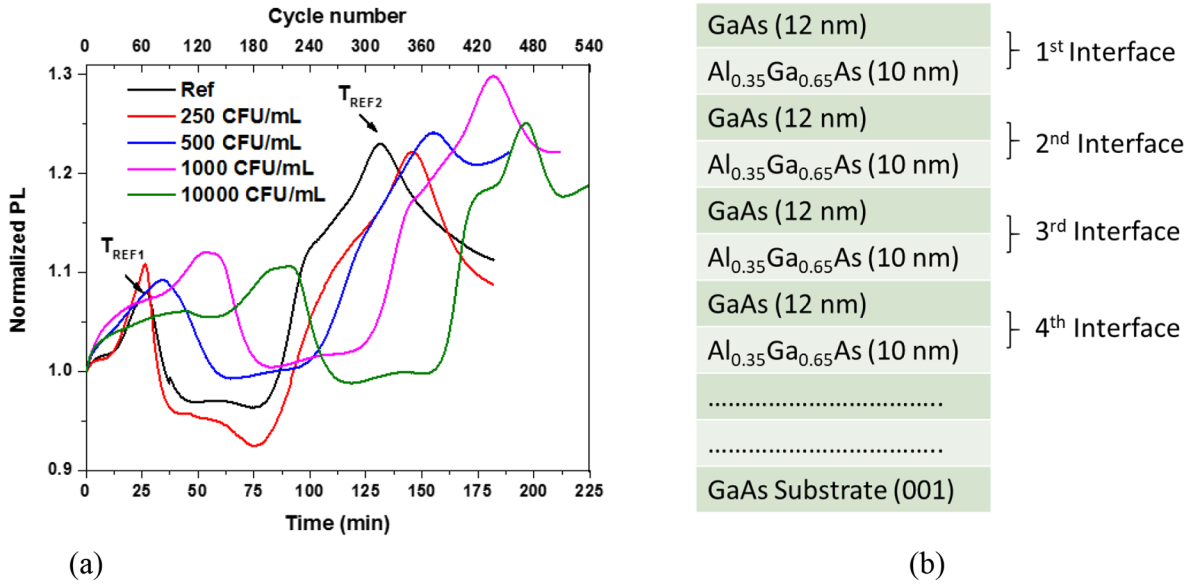

Figure 4. Representative temporal PL intensity plots of GaAs/AlGaAs chips digitally photocorroding (duty cycle = 1.8/25) under a continuous flow of DI water and following the exposure to different concentrations of bacteria (a). Schematic cross section of the investigated GaAs/AlGaAs nanoheterostructure (b).

Table 1. Positions of PL Maxima Observed for DIP GaAs/AlGaAs Chips Exposed to Different Concentrations of Bacteria ($\Delta T_1 = T_1 - T_{REF1}$, $\Delta T_2 = T_2 - T_{REF2}$) and Repeated for Three Different Chips

	first PL maximum (T_1) (min)	second PL maximum (T_2) (min)	ΔT_1 (min)	ΔT_2 (min)
reference	26.66 ± 0.3	130.83 ± 0.3		
250 CFU/mL	26.70 ± 0.3	145.33 ± 0.8	0.00 ± 0.3	14.50 ± 0.8
500 CFU/mL	34.16 ± 0.9	154.58 ± 1.0	7.50 ± 0.9	23.75 ± 1.0
1000 CFU/mL	54.16 ± 1.6	180.83 ± 1.1	27.50 ± 1.6	50.00 ± 1.1
10,000 CFU/mL	86.25 ± 1.6	196.66 ± 1.4	59.59 ± 1.6	65.83 ± 1.4

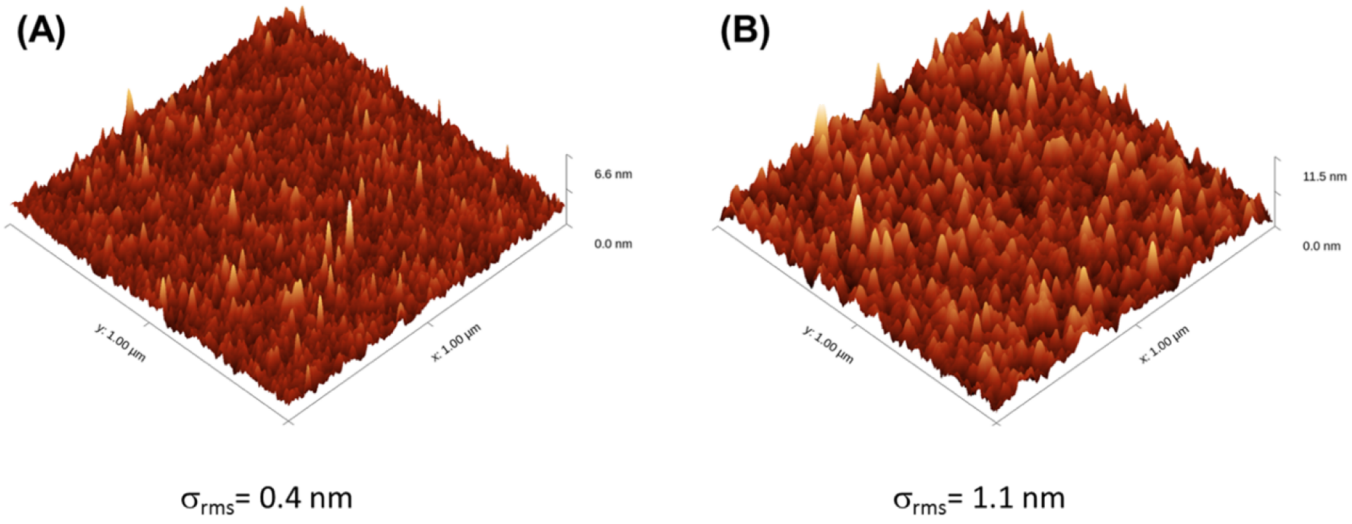

Figure 5. AFM images of a freshly cleaned surface of a GaAs/AlGaAs chip (A) and after exposing the chip to Au−Ab-decorated *E. coli* and 510 cycles of the DIP process that removed two GaAs/AlGaAs bilayers (B).

CFU/mL are shown in Figure 4a. This experiment was carried out with a stack of two pairs of GaAs/$Al_{0.35}Ga_{0.65}As$ nanoheterostructures, whose cross section is schematically shown in Figure 4b. The analysis of the reference and 250 CFU/mL plots shows a negligible difference between the positions of the PL intensity maxima corresponding to photocorrosion of the first pair of the investigated GaAs/AlGaAs nanoheterostructure. However, a 14.5 min delay was observed in the same experiment for the second pair of GaAs/AlGaAs nanoheterostructures, which allowed us to claim the limit of detection (LOD) to be no worse than 250 CFU/mL.

As illustrated in Table 1, systematically greater delay times (ΔT) between the position of PL intensity maxima corresponding to the reference and biosensing runs were observed with the second pair of GaAs/AlGaAs nanolayers for the entire range of investigated bacterial suspensions. This

https://doi.org/10.1021/acs.jpcc.3c05200
J. Phys. Chem. C 2023, 127, 21768−21776

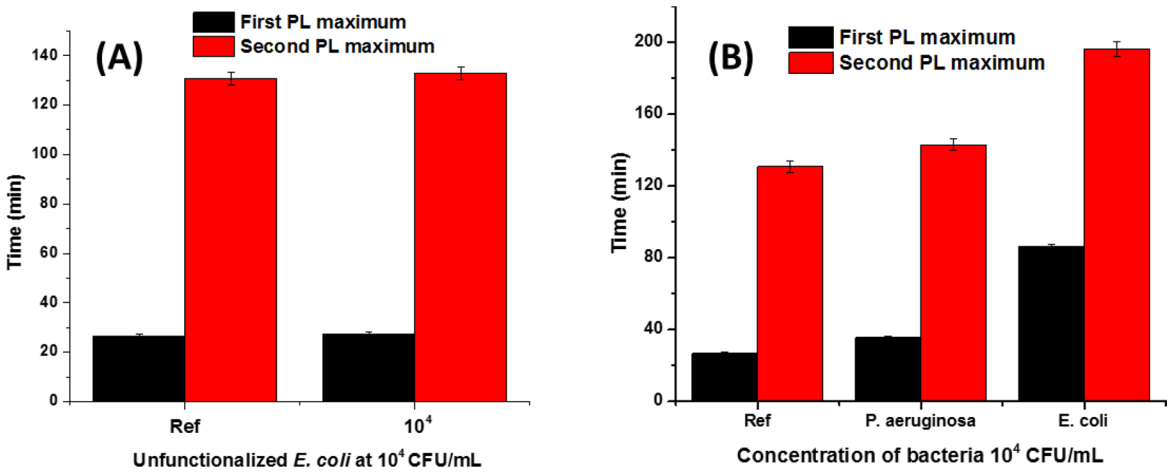

Figure 6. Positions of the first and second PL maximum of the biosensor after exposure to unfunctionalized *E. coli* compared to the reference run (A) and interference study involving *P. aeruginosa* and *E. coli* (B). In both cases, bacterial suspensions are at 10^4 CFU/mL.

illustrates the functioning of an innovative GaAs/AlGaAs DIP biosensor, where the PL intensity maximum revealed for a subsequent GaAs/AlGaAs interface allows the detection of an electrically charged biomolecule (bacteria) with greater precision. This result, however, will depend on the ability to maintain a relatively smooth surface morphology of photocorroding biochips. Figure 5 compares AFM images of a freshly cleaned GaAs/AlGaAs chip (Figure 5a) and a GaAs/AlGaAs nanoheterostructure exposed to functionalized (Ab−Au^{3+}-decorated) *E. coli* at 10^4 CFU/mL and photocorroded to a depth of ∼24 nm, that is, to the bottom of the second AlGaAs layer (Figure 5b).

Indeed, the increase in surface roughness (σ_{RMS}) from 0.4 to 1.1 nm did not prevent the identification of the second GaAs/AlGaAs interface and the successful completion of the biosensing run observed in Figure 4. It is worth mentioning that the roughness of a similar GaAs/AlGaAs nanoheterostructure DIP processed to a depth of 106 nm in a NH_4OH environment was characterized by σ_{RMS} = 0.9 nm.[31] This suggests the possibility of conducting biosensing runs with a greater number of GaAs/AlGaAs nanoheterojunctions, which should be of great interest to designing regenerable DIP biosensing devices.

To confirm that the absorption of bacteria was triggered only by GDR, a GaAs/AlGaAs chip was exposed for 20 min to unfunctionalized *E. coli* at 10^4 CFU/mL, and the PL intensity plots were recorded using the same method as for the reference run. The results presented in Figure 6A indicate negligible differences between the positions of the respective PL maxima, which is consistent with the absence of bacteria on the biochip surface. Thus, the contribution of GDR is indispensable for the immobilization of bacteria on the surface of unfunctionalized GaAs/AlGaAs chips. The specificity of *E. coli* pAbs was investigated by exposing the chip to *P. aeruginosa* functionalized with the same process as that used for capturing *E. coli* and collecting DIP plots. As shown in Figure 6B, *P. aeruginosa* at 10^4 CFU/mL did not significantly shift the position of the PL intensity maximum compared to the PL reference run. This confirmed the relative specificity of the investigated antibodies and ruled out the possibility of meaningful interference by different bacterial strains.

The construction of a calibration plot was based on *E. coli* suspensions in PBS at 250−10,000 CFU/mL. In each case, bacterial suspensions were exposed for 20 min to 80 μg/mL for gold-conjugated antibodies, and after centrifugation, the produced pellets were diluted in 1 mL of PBS. Figure 7

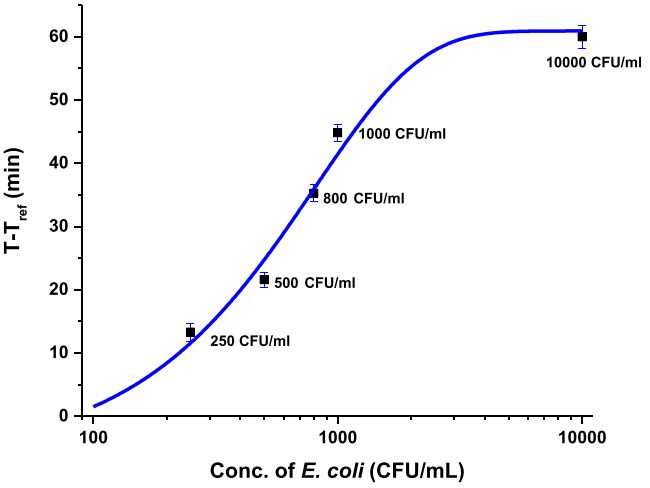

Figure 7. Calibration curve based on the position of the second PL intensity maximum revealed with the digital photocorrosion process of GaAs (12 nm)/AlGaAs (10 nm) nanoheterostructures. The position of a reference PL maximum was determined with the error not exceeding ±3 min (Wafer D3422).

shows the results of the DIP-determined delayed positions of the second PL intensity maxima of the unfunctionalized GaAs/AlGaAs biochips with respect to the reference run. The results, repeated three times, revealed clear $T-T_{ref}$ differences with an LOD as low as 250 CFU/mL (see Figure S4 for a bar graph corresponding to these results).

It is relevant to mention that the excessive concentration of gold ions on the bacterial surface can accelerate the photocorrosion of GaAs/AlGaAs nanoheterostructures. This is due to two phenomena that occur simultaneously: (i) accelerated photocorrosion induced by the spontaneous electron transfer between GaAs and Au^{3+} and (ii) reduced photocorrosion rate due to reduced band bending induced by the absorption of electron-donating species (bacteria), which weakens the electric field driving holes toward the semiconductor surface. For instance, a significantly accelerated DIP process was observed for *E. coli* following exposure to a

https://doi.org/10.1021/acs.jpcc.3c05200
J. Phys. Chem. C 2023, 127, 21768−21776

solution of Au^{3+} ions at a concentration increased to 2 mM (see Figure S5 in Supporting Information). Although research on the threshold concentration of Au^{3+} required for the successful immobilization of bacteria may still be warranted, we argue that the biosensing reaction of GaAs/AlGaAs biochips to trace amounts of ionic gold (1 mM) employed in this report for the decoration of bacteria is an attractive illustration of the proposed biosensing methodology.

5. CONCLUSIONS

We have investigated an innovative method for detecting bacteria (*E. coli*) decorated with antibodies and Au^{3+} ions that transform into Au^0 nanoparticles upon contact with the surface of a III−V semiconductor (GaAs/AlGaAs nanoheterostructures). The galvanic displacement reaction responsible for this process offers robust immobilization of bacteria owing to the formation of the interfacial Au−Ga alloy between the semiconductor and Au-decorated (functionalized) bacteria. From the delay of the digital photocorrosion process of GaAs/AlGaAs nanoheterostructures induced by the transfer of an extra negative charge from the bacteria to the biochip surface, the method allowed rapid detection of *E. coli* in suspensions from 2.5×10^2 to the maximum tested at 10^4 CFU/mL. The LOD at 2.5×10^2 CFU/mL was achieved by monitoring the delay of the digital photocorrosion process of the second pair of GaAs/AlGaAs nanoheterostructures. Our results suggest that further enhanced LOD should be possible by considering digital photocorrosion of the third or deeper located pairs of GaAs/AlGaAs layers. Galvanic displacement-based biosensing that employs digitally photocorroding III−V nanoheterostructures is attractive, also because of the elimination of the chip biofunctionalization procedure. Ultimately, this approach is potentially attractive for the development of technology of regenerable biosensors employing stacks of semiconductor nanolayers for quasi-continuous monitoring of the environment for the presence of pathogenic biomolecules.

■ ASSOCIATED CONTENT

Supporting Information

The Supporting Information is available free of charge at https://pubs.acs.org/doi/10.1021/acs.jpcc.3c05200.

Standard operation procedure for the functionalization of *E. coli* (Figure S1); XPS scan of the GaAs/AlGaAs nanoheterostructure after the absorption of Au^{3+}-coated bacteria (Figure S2); FTIR spectra of GaAs/AlGaAs biosensors after physical adsorption of bacteria and specific immobilization of Au^{3+}-antibody-functionalized bacteria (Figure S3); a bar graph with delay times of PL intensity maxima for reference and biosensing runs observed with the first and second PL maxima for bacteria decorated in a 1 mM Au^{3+} ionic solution (Figure S4); biosensing plots and bar graphs for the reference and biosensing runs observed for bacteria decorated with an excess concentration of Au^{3+} ions obtained from a 2 mM Au^{3+} solution (Figure S5) (PDF)

■ AUTHOR INFORMATION

Corresponding Author

Jan J. Dubowski − *Laboratory for Quantum Semiconductors and Photon-Based BioNanotechnology, Interdisciplinary Institute for Technological Innovation (3IT), CNRS IRL-3463, Department of Electrical and Computer Engineering, Université de Sherbrooke, Sherbrooke, Québec J1K 0A5, Canada*; orcid.org/0000-0003-0022-527X; Email: jan.j.dubowski@usherbrooke.ca

Authors

Amanpreet Singh − *Laboratory for Quantum Semiconductors and Photon-Based BioNanotechnology, Interdisciplinary Institute for Technological Innovation (3IT), CNRS IRL-3463, Department of Electrical and Computer Engineering, Université de Sherbrooke, Sherbrooke, Québec J1K 0A5, Canada*

Walid M. Hassen − *Laboratory for Quantum Semiconductors and Photon-Based BioNanotechnology, Interdisciplinary Institute for Technological Innovation (3IT), CNRS IRL-3463, Department of Electrical and Computer Engineering, Université de Sherbrooke, Sherbrooke, Québec J1K 0A5, Canada*

René St-Onge − *Laboratory for Quantum Semiconductors and Photon-Based BioNanotechnology, Interdisciplinary Institute for Technological Innovation (3IT), CNRS IRL-3463, Department of Electrical and Computer Engineering, Université de Sherbrooke, Sherbrooke, Québec J1K 0A5, Canada*

Complete contact information is available at: https://pubs.acs.org/10.1021/acs.jpcc.3c05200

Author Contributions

Conceptualization and investigation, A.S. and J.J.D.; methodology, A.S. and W.M.H.; formal analysis, A.S., W.M.H., and R.S.-O.; writing—original draft preparation, A.S.; writing—review and editing, A.S., W.M.H., and J.J.D.; supervision, project administration, and funding acquisition, J.J.D. All authors have read and agreed to the published version of the manuscript.

Notes

The authors declare no competing financial interest.

■ ACKNOWLEDGMENTS

This work was supported by the Natural Sciences and Engineering Research Council of Canada (NSERC) discovery grant RGPIN-2020-05558. A.S. acknowledges the FRQNT Merit Scholarship for Foreign Students (PBEEE; Québec, Canada). The authors are indebted to Patricia Moraille (Université de Montréal) for collecting the AFM-IR data and Sonia Blais (Université de Sherbrooke) for collecting the XPS data. The assistance of Jonathan Vermette (3IT) in collecting the FTIR data is also acknowledged.

■ REFERENCES

(1) Kotlarz, N.; Rockey, N.; Olson, T. M.; Haig, S. J.; Sanford, L.; LiPuma, J. J.; Raskin, L. Biofilms in Full-Scale Drinking Water Ozone Contactors Contribute Viable Bacteria to Ozonated Water. *Environ. Sci. Technol.* **2018**, *52* (5), 2618−2628.

(2) Wang, J.; Lu, J.; Zhou, Y.; Zhou, Y. Multifunctional Antibacterial Materials for the Control of Hazardous Microbes and Chemicals: A Review. *ACS ES&T Water* **2021**, *1* (3), 479−497.

(3) Malakar, P.; Mukherjee, A.; Bhanja, S. N.; Sarkar, S.; Saha, D.; Ray, R. K. Deep Learning-Based Forecasting of Groundwater Level Trends in India: Implications for Crop Production and Drinking Water Supply. *ACS ES&T Engineering* **2021**, *1* (6), 965−977.

(4) Angus, D. C.; van der Poll, T. Severe Sepsis and Septic Shock. *New England Journal of Medicine* **2013**, *369* (9), 840−851.

(5) Taylor, L. H.; Levin, B. R.; Antia, R. Why we don't get sick: the within-host population dynamics of bacterial infections. *Science* **2001**, *292* (5519), 1112−1115.
(6) Katayev, E. A.; Pantos, G. D.; Reshetova, M. D.; Khrustalev, V. N.; Lynch, V. M.; Ustynyuk, Y. A.; Sessler, J. L. Anion-induced synthesis and combinatorial selection of polypyrrolic macrocycles. *Angew. Chem., Int. Ed. Engl.* **2005**, *44* (45), 7386−7390.
(7) Zhu, T.; Liu, H.; Su, L.; Xiong, X.; Wang, J.; Xiao, Y.; Zhu, Y.; Peng, Y.; Dawood, A.; Hu, C.; et al. MicroRNA-18b-5p Down-regulation Favors Mycobacterium tuberculosis Clearance in Macrophages via HIF-1alpha by Promoting an Inflammatory Response. *ACS Infect Dis* **2021**, *7* (4), 800−810.
(8) Nukaga, M.; Yoon, M. J.; Taracilia, M. A.; Hoshino, T.; Becka, S. A.; Zeiser, E. T.; Johnson, J. R.; Papp-Wallace, K. M. Assessing the Potency of beta-Lactamase Inhibitors with Diverse Inactivation Mechanisms against the PenA1 Carbapenemase from Burkholderia multivorans. *ACS Infect Dis* **2021**, *7* (4), 826−837.
(9) Rocamora, F.; Gupta, P.; Istvan, E. S.; Luth, M. R.; Carpenter, E. F.; Kumpornsin, K.; Sasaki, E.; Calla, J.; Mittal, N.; Carolino, K.; et al. PfMFR3: A Multidrug-Resistant Modulator in Plasmodium falciparum. *ACS Infect Dis* **2021**, *7* (4), 811−825.
(10) Duvall, S. W.; Childers, W. S. Design of a Histidine Kinase FRET Sensor to Detect Complex Signal Integration within Living Bacteria. *ACS Sens* **2020**, *5* (6), 1589−1596.
(11) Furst, A. L.; Francis, M. B. Impedance-Based Detection of Bacteria. *Chem. Rev.* **2019**, *119* (1), 700−726.
(12) Lepage, D.; Jimenez, A.; Beauvais, J.; Dubowski, J. J. Conic hyperspectral dispertion mapping. *Light: Science and Applications* **2012**, *1*, No. e28.
(13) Chernov, K. G.; Redchuk, T. A.; Omelina, E. S.; Verkhusha, V. V. Near-Infrared Fluorescent Proteins, Biosensors, and Optogenetic Tools Engineered from Phytochromes. *Chem. Rev.* **2017**, *117* (9), 6423−6446.
(14) Yang, S.; Wen, W. Lyophilized Ready-to-Use Mix for the Real-Time Polymerase Chain Reaction Diagnosis. *ACS Appl. Bio Mater.* **2021**, *4* (5), 4354−4360.
(15) Veedu, R. N.; Vester, B.; Wengel, J. Polymerase chain reaction and transcription using locked nucleic acid nucleotide triphosphates. *J. Am. Chem. Soc.* **2008**, *130* (26), 8124−8125.
(16) Canalle, L. A.; Vong, T.; Adams, P. H.; van Delft, F. L.; Raats, J. M.; Chirivi, R. G.; van Hest, J. C. Clickable enzyme-linked immunosorbent assay. *Biomacromolecules* **2011**, *12* (10), 3692−3697.
(17) Xing, K. Y.; Peng, J.; Shan, S.; Liu, D. F.; Huang, Y. N.; Lai, W. H. Green Enzyme-Linked Immunosorbent Assay Based on the Single-Stranded Binding Protein-Assisted Aptamer for the Detection of Mycotoxin. *Anal. Chem.* **2020**, *92* (12), 8422−8426.
(18) He, Z.; Huffman, J.; Curtin, K.; Garner, K. L.; Bowdridge, E. C.; Li, X.; Nurkiewicz, T. R.; Li, P. Composable Microfluidic Plates (cPlate): A Simple and Scalable Fluid Manipulation System for Multiplexed Enzyme-Linked Immunosorbent Assay (ELISA). *Anal. Chem.* **2021**, *93* (3), 1489−1497.
(19) Maley, A. M.; Garden, P. M.; Walt, D. R. Simplified Digital Enzyme-Linked Immunosorbent Assay Using Tyramide Signal Amplification and Fibrin Hydrogels. *ACS Sens* **2020**, *5* (10), 3037−3042.
(20) Rahi, P.; Prakash, O.; Shouche, Y. S. Matrix-Assisted Laser Desorption/Ionization Time-of-Flight Mass-Spectrometry (MALDI-TOF MS) Based Microbial Identifications: Challenges and Scopes for Microbial Ecologists. *Front. Microbiol.* **2016**, *7*, 1359.
(21) Jung, H.; Park, S. H.; Lee, J.; Lee, B.; Park, J.; Seok, Y.; Choi, J. H.; Kim, M. G.; Song, C. S.; Lee, J. A Size-Selectively Biomolecule-Immobilized Nanoprobe-Based Chemiluminescent Lateral Flow Immunoassay for Detection of Avian-Origin Viruses. *Anal. Chem.* **2021**, *93* (2), 792−800.
(22) Soler, M.; Estevez, M. C.; Cardenosa-Rubio, M.; Astua, A.; Lechuga, L. M. How Nanophotonic Label-Free Biosensors Can Contribute to Rapid and Massive Diagnostics of Respiratory Virus Infections: COVID-19 Case. *ACS Sens* **2020**, *5*, 2663−2678.
(23) Grant, B. D.; Anderson, C. E.; Williford, J. R.; Alonzo, L. F.; Glukhova, V. A.; Boyle, D. S.; Weigl, B. H.; Nichols, K. P. SARS-CoV-2 Coronavirus Nucleocapsid Antigen-Detecting Half-Strip Lateral Flow Assay Toward the Development of Point of Care Tests Using Commercially Available Reagents. *Anal. Chem.* **2020**, *92* (16), 11305−11309.
(24) Zhang, C.; Zheng, T.; Wang, H.; Chen, W.; Huang, X.; Liang, J.; Qiu, L.; Han, D.; Tan, W. Rapid One-Pot Detection of SARS-CoV-2 Based on a Lateral Flow Assay in Clinical Samples. *Anal. Chem.* **2021**, *93* (7), 3325−3330.
(25) Shan, B.; Broza, Y. Y.; Li, W.; Wang, Y.; Wu, S.; Liu, Z.; Wang, J.; Gui, S.; Wang, L.; Zhang, Z.; et al. Multiplexed Nanomaterial-Based Sensor Array for Detection of COVID-19 in Exhaled Breath. *ACS Nano* **2020**, *14* (9), 12125−12132.
(26) Kaushik, A. K.; Dhau, J. S.; Gohel, H.; Mishra, Y. K.; Kateb, B.; Kim, N. Y.; Goswami, D. Y. Electrochemical SARS-CoV-2 Sensing at Point-of-Care and Artificial Intelligence for Intelligent COVID-19 Management. *ACS Appl. Bio Mater.* **2020**, *3* (11), 7306−7325.
(27) Parihar, A.; Ranjan, P.; Sanghi, S. K.; Srivastava, A. K.; Khan, R. Point-of-Care Biosensor-Based Diagnosis of COVID-19 Holds Promise to Combat Current and Future Pandemics. *ACS Applied Bio Materials* **2020**, *3* (11), 7326−7343.
(28) Cesewski, E.; Johnson, B. N. Electrochemical biosensors for pathogen detection. *Biosens. Bioelectron.* **2020**, *159*, No. 112214.
(29) Sharma, A.; Mishra, R. K.; Goud, K. Y.; Mohamed, M. A.; Kummari, S.; Tiwari, S.; Li, Z.; Narayan, R.; Stanciu, L. A.; Marty, J. L. Optical Biosensors for Diagnostics of Infectious Viral Disease: A Recent Update. *Diagnostics* **2021**, *11*, 2083.
(30) Samota, S.; Rani, R.; Chakraverty, S.; Kaushik, A. Biosensors for simplistic detection of pathogenic bacteria: A review with special focus on field-effect transistors. *Materials Science in Semiconductor Processing* **2022**, *141*, No. 106404.
(31) Aziziyan, M. R.; Hassen, W. M.; Sharma, H.; Shirzaei Sani, E.; Annabi, N.; Frost, E. H.; Dubowski, J. J. Sodium dodecyl sulfate decorated Legionella pneumophila for enhanced detection with a GaAs/AlGaAs nanoheterostructure biosensor. *Sens. Actuators, B* **2020**, *304*, No. 127007.
(32) Nazemi, E.; Hassen, W. M.; Frost, E. H.; Dubowski, J. J. Monitoring growth and antibiotic susceptibility of Escherichia coli with photoluminescence of GaAs/AlGaAs quantum well microstructures. *Biosens Bioelectron* **2017**, *93*, 234−240.
(33) Islam, M. A.; Hassen, W. M.; Tayabali, A. F.; Dubowski, J. J. Short Ligand, Cysteine-Modified Warnericin RK Antimicrobial Peptides Favor Highly Sensitive Detection of Legionella pneumophila. *ACS Omega* **2021**, *6* (2), 1299−1308.
(34) Aziziyan, M. R.; Sharma, H.; Dubowski, J. J. Photo-Atomic Layer Etching of GaAs/AlGaAs Nanoheterostructures. *ACS Appl. Mater. Interfaces* **2019**, *11* (19), 17968−17978.
(35) Aithal, S.; Dubowski, J. J. Open circuit potential monitored digital photocorrosion of GaAs/AlGaAs quantum well microstructures. *Appl. Phys. Lett.* **2018**, *112* (15), 153102.
(36) Nazemi, E.; Aithal, S.; Hassen, W. M.; Frost, E. H.; Dubowski, J. J. GaAs/AlGaAs heterostructure based photonic biosensor for rapid detection of Escherichia coli in phosphate buffered saline solution. *Sens. Actuators, B* **2015**, *207*, 556−562.
(37) Aziziyan, M. R.; Hassen, W. M.; Morris, D.; Frost, E. H.; Dubowski, J. J. photonic biosensor based on photocorrosion of GaAs/AlGaAs quantum heterostructures for detection of Legionella pneumophila. *Biointerphases* **2016**, *11* (1), No. 019301.
(38) Islam, M. A.; Hassen, W. M.; Tayabali, A. F.; Dubowski, J. J. Antimicrobial warnericin RK peptide functionalized GaAs/AlGaAs biosensor for highly sensitive and selective detection of Legionella pneumophila. *Biochemical Engineering Journal* **2020**, *154*, No. 107435.
(39) Lepage, D.; Jimenez, A.; Beauvais, J.; Dubowski, J. J. Real-time detection of influenza A virus using semiconductor nanoplasmonics. *Light: Science and Applications* **2013**, *2* (e62), No. e62.
(40) Marquez, D. T.; Chawich, J.; Hassen, W. M.; Moumanis, K.; DeRosa, M. C.; Dubowski, J. J. Polymer Brush−GaAs Interface and

https://doi.org/10.1021/acs.jpcc.3c05200
J. Phys. Chem. C 2023, 127, 21768−21776

Its Use as an Antibody-Compatible Platform for Biosensing. *ACS Omega* **2021**, *6* (11), 7286−7295.
(41) Aithal, S.; Liu, N.; Dubowski, J. J. Photocorrosion metrology of photoluminescence emitting GaAs/AlGaAs heterostructures. *J. Phys. D: Appl. Phys.* **2017**, *50* (3), No. 035106.
(42) Kim, S. J.; Seong, M.; Yun, H. W.; Ahn, J.; Lee, H.; Oh, S. J.; Hong, S. H. Chemically Engineered Au-Ag plasmonic Nanostructures to Realize Large Area and Flexible Metamaterials. *ACS Appl. Mater. Interfaces* **2018**, *10* (30), 25652−25659.
(43) Aizawa, M.; Buriak, J. M. Block Copolymer Templated Chemistry for the Formation of Metallic Nanoparticle Arrays on Semiconductor Surfaces. *Chem. Mater.* **2007**, *19* (21), 5090−5101.
(44) Sarkar, A.; Manthiram, A. Synthesis of Pt@Cu Core−Shell Nanoparticles by Galvanic Displacement of Cu by Pt^{4+} Ions and Their Application as Electrocatalysts for Oxygen Reduction Reaction in Fuel Cells. *J. Phys. Chem. C* **2010**, *114* (10), 4725−4732.
(45) Singh, A.; St-Onge, R.; Dubowski, J. J. Consequence of Galvanic Displacement Reaction on Digital Photocorrosion of GaAs/Al0.35Ga0.65As Nanoheterostructures. *J. Phys. Chem. C* **2020**, *124* (50), 27772−27779.
(46) Aizawa, M.; Buriak, J. M. Block copolymer-templated chemistry on Si, Ge, InP, and GaAs surfaces. *J. Am. Chem. Soc.* **2005**, *127* (25), 8932−8933.
(47) Sayed, S. Y.; Daly, B.; Buriak, J. M. Characterization of the Interface of Gold and Silver Nanostructures on InP and GaAs Synthesized via Galvanic Displacement. *J. Phys. Chem. C* **2008**, *112* (32), 12291−12298.
(48) Singh, A.; Bains, D.; Hassen, W. M.; Singh, N.; Dubowski, J. J. Formation of a Au/Au_9Ga_4 Alloy Nanoshell on a Bacterial Surface through Galvanic Displacement Reaction for High-Contrast Imaging. *ACS Applied Bio Materials* **2020**, *3* (1), 477−485.
(49) Vanysek, P. Electrochemical Series. In *Handbook of Chemistry and Physics*; 92nd ed.; Haynes, W. M., Ed.; Chemical Rubber Company: Boca Raton, 2011; pp 5−80, 85−82.
(50) Dave, N.; Troullier, A.; Mus-Veteau, I.; Dunach, M.; Leblanc, G.; Padros, E. Secondary structure components and properties of the melibiose permease from Escherichia coli: a fourier transform infrared spectroscopy analysis. *Biophys. J.* **2000**, *79* (2), 747−755.
(51) Onodera, K.; Hirano-Iwata, A.; Miyamoto, K. I.; Kimura, Y.; Kataoka, M.; Shinohara, Y.; Niwano, M. Label-free detection of protein-protein interactions at the GaAs/Water interface through surface infrared spectroscopy: Discrimination between specific and nonspecific interactions by using secondary structure analysis. *Langmuir* **2007**, *23* (24), 12287−12292.
(52) Nadtochenko, V. A.; Rincon, A. G.; Stanca, S. E.; Kiwi, J. Dynamics of E. coli membrane cell peroxidation during TiO_2 photocatalysis studied by ATR-FTIR spectroscopy and AFM microscopy. *J. Photochem. Photobiol., A* **2005**, *169* (2), 131−137.
(53) Kamnev, A. A.; Dykman, L. A.; Tarantilis, P. A.; Polissiou, M. G. Spectroimmunochemistry using colloidal gold bioconjugates. *Biosci Rep* **2002**, *22* (5−6), 541−547.

https://doi.org/10.1021/acs.jpcc.3c05200
J. Phys. Chem. C 2023, 127, 21768−21776